Quasiperiodic Emissions and Related Particle Precipitation Bursts Observed by the DEMETER Spacecraft

František Němec, M. Hajoš, Michel Parrot, O. Santolík

Quasiperiodic Emissions and Related Particle Precipitation Bursts Observed by the DEMETER Spacecraft

F. Němec[1], M. Hajoš[2], M. Parrot[3], O. Santolík[2,1]

[1]Faculty of Mathematics and Physics, Charles University, Prague, Czech Republic
[2]Department of Space Physics, Institute of Atmospheric Physics of the Czech Academy of Sciences, Prague, Czech Republic
[3]LPC2E/CNRS, Orléans, France

Key Points:

- Energetic electron precipitation bursts corresponding to quasiperiodic emission peaks are identified.
- Interaction regions occur at L-shells between about 4 and 6 and have dimensions of about 0.6 to 1.2 Earth radii.
- Individual wave elements exhibit a fine inner structure corresponding to the wave bouncing between the hemispheres.

Corresponding author: František Němec, `frantisek.nemec@mff.cuni.cz`

Abstract

Electromagnetic waves observed in the inner magnetosphere at frequencies between about 0.5 and 4 kHz sometimes exhibit a quasiperiodic (QP) time modulation of the wave intensity with modulation periods from tens of seconds up to a few minutes. Such waves are typically termed QP emissions and their origin is still not fully understood. We use a large set of more than 2,000 of these events identified in the low-altitude DEMETER spacecraft data to check for energetic electron flux variations matching the individual QP wave elements. Altogether, 7 such events are identified and their detailed analysis is performed. Energetic electron fluxes are found to be modulated primarily at energies lower than about 250 keV. While the waves may propagate unducted across L-shells, the energetic particles follow magnetic field lines from the interaction region down to the observation point. This is used to estimate the locations of anticipated generation regions to L-shells between about 4 and 6, and the respective source radial dimensions to about 0.6–1.2 Earth radii. The frequencies of the events are confined below half of the equatorial electron gyrofrequency in the determined source regions. Finally, it is shown that individual QP elements exhibit a fine inner structure corresponding to the wave bouncing between the hemispheres.

1 Introduction

Inner magnetospheric whistler mode waves at frequencies between about 0.5 and 4 kHz sometimes exhibit a nearly periodic time modulation of the wave intensity. The modulation period can range from tens of seconds up to a few minutes, and the respective emissions are typically called quasiperiodic (QP) emissions. Although they have been known already for a few decades (Carson et al., 1965), their origin is still not fully understood, and neither are their generation locations. Two principally different generation mechanisms have been considered. First, it has been suggested that the QP modulation may be a result of the source region being periodically modulated by a compressional ultra low frequency (ULF) wave with a period corresponding to the period of the QP modulation (Chen, 1974; Kimura, 1974; Sazhin, 1987). Second, a flow cyclotron maser mechanism able to self-consistently explain the origin of the QP modulation even without the presence of the ULF magnetic field pulsations has been proposed (Demekhov & Trakhtengerts, 1994; Pasmanik, Demekhov, et al., 2004). As for the supporting experimental evidence, some of the observed QP events appear to be more or less clearly related to the ULF pulsations (Sato & Kokubun, 1981), while for many events such pulsations are missing and the flow cyclotron maser mechanism is able to reproduce their basic characteristics and dependences (Pasmanik, Titova, et al., 2004; Pasmanik et al., 2019). It seems well possible that both mechanisms are eventually plausible, depending on the conditions and event properties. Historically, the events related to the ULF pulsations were classified as QP events type 1, while the other events were classified as QP events type 2 (Kitamura et al., 1969; Sato et al., 1974). This latter class might be related to the flow cyclotron maser mechanism. Even though such event classification seems problematic at least (Tixier & Cornilleau-Wehrlin, 1986; Sazhin & Hayakawa, 1994), Bezděková et al. (2019) demonstrated that the QP events indeed appear to form two different classes based on their properties and dependences on the solar wind parameters.

A survey of QP event observations by the Van Allen Probes spacecraft revealed that the events occur primarily, but not exclusively, inside the plasmasphere (Němec et al., 2018). Although the planarities of the wave magnetic field fluctuations (Santolík et al., 2003) are typically rather low, indicating a mixture of waves coming to the spacecraft from different directions, the waves are found to propagate mostly away from the geomagnetic equator. This suggests that the events are indeed generated in the equatorial region, which is a preferred region for wave-particle interactions in general (Trakhtengerts & Rycroft, 2008), and has been formerly suggested as a possible source location of the emissions (Sato & Kokubun, 1980; Morrison, 1990). The observed oblique wave normal angles demonstrate that the wave propagation is primarily unducted (Martinez-Calderon et al., 2016; Němec et al., 2018). The unducted propagation is believed to be responsible for the same QP modulation being observed over comparatively large regions of space (Němec, Santolík, Parrot, et al., 2013; Němec, Hospodarsky, et al., 2016; Němec, Bezděková, et al., 2016; Bezděková et al., 2020). This is supported by multipoint measurements and detailed time delay analysis, which reveals a time delay on the order of seconds between different locations (Němec et al., 2014; Martinez-Calderon et al., 2016). A plasmapause guiding (Hayosh et al., 2016) and ionospheric reflections (Hanzelka et al., 2017) may be further important for the propagation of QP emissions down to low altitudes. Ground-based measurements then, in turn, enable observations of a given event for an extensive period of time (Manninen et al., 2012). They were used to reveal variations of QP modulation periods related to substorms (Manninen et al., 2013; Manninen, Titova, et al., 2014). While both ground-based (Morrison et al., 1994; A. J. Smith et al., 1998; Engebretson et al., 2004) and low-altitude spacecraft (Hayosh et al., 2014) surveys suggested that QP emissions are primarily daytime phenomenon, satellite surveys at larger radial distances revealed the emissions essentially at all local times (Němec, Santolík, Pickett, et al., 2013; Němec et al., 2018). This apparent inconsistency can be explained by significant lightning-related background wave intensities which may obscure the events at low altitudes (Němec et al., 2020).

Quasiperiodic variations of energetic electron precipitation related to the event occurrence and related ionospheric changes were suggested as a possible explanation for concurrent magnetic field pulsations observed on the ground (Sato & Matsudo, 1986). More recently, Hayosh et al. (2013) presented a case study of energetic electron flux variations corresponding to individual QP wave elements observed by the low-altitude DEMETER spacecraft. Titova et al. (2015) used Van Allen Probes spacecraft measurements to identify energetic electron flux changes with periods corresponding to the QP modulation in the proximity of a tentative source region. Finally, Li et al. (2021) used simultaneous measurements of QP emissions by the Van Allen Probes and energetic electron precipitation by the low-altitude POES satellite to demonstrate energetic electron precipitation in association with QP emissions.

In the present study, QP electromagnetic wave events observed by the DEMETER spacecraft during its entire mission identified by Hayosh et al. (2014) are used to check for energetic electron flux variations matching the wave intensity modulations. This provides us with the information about the magnetic field lines containing tentative event source regions. A brief overview of the used data set is given in section 2. The results obtained are presented in section 3 and they are discussed in section 4. Finally, section 5 contains a brief summary of the main results.

2 Data

DEMETER was a French low-altitude satellite operating between 2004 and 2010 at an altitude of about 700 km. The spacecraft measurements were performed nearly continuously at geomagnetic latitudes below about 65 degrees, while principally no measurements came from larger latitudes. The spacecraft orbit was nearly Sun-synchronous, resulting in the measurements being performed either close to the local noon (about 10:30 LT, "daytime") or close to the local midnight (about 22:30 LT, "nighttime"). Out of the instruments onboard, the electric field instrument (ICE), the magnetic field instrument (IMSC), and the energetic particle detector (IDP) are used in the present study. Two different modes of the spacecraft operation were possible, called "Burst" and "Survey". During the continuously active Survey mode, lower resolution data were measured. The Survey mode electric field measurements in the very low frequency range consisted of onboard calculated frequency spectra of a single electric field component with the frequency resolution of about 20 Hz and the time resolution of about 2 s. The Survey mode energetic particle data consisted of two different data products. First, the total energetic electron fluxes in three energy ranges (90.7–526.8 keV, 526.8–971.8 keV, and 971.8–2342.4 keV) were measured with a time resolution of 1 s. Second, the energetic electron spectra with 128 linearly spaced energy channels spanning between 72.9 and 2333.5 keV were measured with a time resolution of 4 s. The Burst mode was active only during specifically selected time intervals, providing some higher resolution data on top of the normal Survey mode data. During this mode, a waveform of a single electric field component sampled at 40 kHz and waveforms of all six electromagnetic field components sampled at 2.5 kHz are available. Due to a significant number of interferences in the magnetic field data at frequencies between about 1 and 8 kHz, this is the only data product of the magnetic field instrument that is used. Additionally, energetic electron spectra have better energy (256 energy channels instead of 128) and time resolution (1 s in place of 4 s). More detailed description of the ICE, IMSC, and IDP instruments is given by Berthelier et al. (2006), Parrot et al. (2006) and Sauvaud et al. (2006), respectively.

A starting point of our analysis is a list of all QP events observed during the entire duration of the DEMETER mission compiled by Hayosh et al. (2014). Altogether, the list consists of as many as 2,264 events. Out of that, 2,181 events occurred during the daytime, while only 83 events were identified during the nighttime. The list provides a beginning and ending times, as well as lowest and highest frequencies of all the events. For each event separately, these are used to plot the respective frequency-time spectrograms of power spectral densities of electric field fluctuations. Additionally, the time dependences of total energetic electron fluxes in the lowest of the three survey mode energy ranges are plotted using the same temporal scale. Individual plots are then visually investigated for the presence of energetic electron flux peaks at the times of the individual QP elements. In order to eliminate possible random coincidences, it is required that the electron flux is noticeably increased at the times of at least three consecutive

Figure 1. Example of a quasiperiodic event with simultaneous energetic electron precipitation bursts. (a) Frequency-time spectrogram of power spectral density of electric field fluctuations. (b) Energy-time plot of measured energetic electron fluxes. (c) Average power spectral density of electric field fluctuations in the frequency range between 1200 and 1900 Hz, corresponding to the event, is shown by the black curve. The red curve shows total energetic electron flux in the energy range between about 90 and 525 keV. The vertical dashed lines mark the time interval where the wave elements are accompanied by increased particle fluxes.

QP elements. Altogether, 7 events fulfilling this condition are identified, all during the daytime. Geomagnetic activity conditions during the 7 events do not appear to be exceptional in any way as compared to the geomagnetic activity conditions for the entire DEMETER QP event list.

3 Results

An example of one of the identified events where a QP event is accompanied by corresponding quasiperiodic bursts in energetic electron fluxes is shown in Figure 1. The event occurred on 24 October 2006. The plotted time interval starts in the beginning of data acquisition during the given orbit. Figure 1a shows a frequency-time spectrogram of power spectral density of electric field fluctuations corresponding to the QP event. Individual QP elements with the intensity gradually decreasing toward lower geomagnetic latitudes (later times) can be seen. The white vertical bars correspond to short data gaps related to turning on/off the Burst mode measurements, i.e., the Burst mode data are available in the time interval marked by the vertical white bars.

Figure 1b shows energy-time plot of measured energetic electron fluxes. Several peaks of enhanced fluxes are identifiable at the lowest energies close to the beginning of the plotted time interval. The peaks in the wave intensity and measured energetic electron fluxes are analyzed more in detail in Figure 1c, which shows the respective time dependences. The black curve shows the time dependence of the average power spectral density in the frequency range between 1200 and 1900 Hz, where the core of the QP event occurs. The red curve shows the time dependence of the measured energetic electron flux corresponding to the lowest energy count channel, i.e., approximately between about 90 and 525 keV. The periodic modulation of both the wave intensity and energetic electron fluxes can be

Figure 2. Zoom of the time interval marked by the dashed vertical lines in Figure 1. The vertical dashed lines mark the approximate times of wave intensity/energetic electron flux peaks.

Figure 3. L-shell ranges where individual events are observed in (red) energetic electron data and (black) wave intensity.

Figure 4. (a) Histogram of L-shell values where the analyzed events are observed in (red) energetic electron data and (black) wave intensity. (b) Histogram of radial extents of determined source dimensions.

clearly seen. While the wave intensity exhibits a QP modulation principally all over the plotted time interval, the QP modulation of the energetic electron fluxes is limited to the time interval shortly after the beginning of the plot. This time interval is marked by the vertical dashed lines. The individual peaks of energetic electron fluxes in this time interval occur approximately at the same times as the peaks of the wave intensity. Note that the huge increase of the electron flux seen in Figure 1c at later times (about 15:35 UT) corresponds to the slot region.

A more detailed view of the time interval marked by the dashed vertical lines is shown in Figure 2 using a format analogous to the one used in Figure 1. The vertical dashed lines mark the times of five wave intensity peaks identified in Figure 2a. As demonstrated by Figure 2c, the marked times correspond well also to the peaks in measured energetic electron fluxes. Some of the energetic electron flux peaks are identifiable also in the energy spectrum plot in Figure 2b, although they are quite obscured due to the lower time resolution of the data and the used color coding representation.

A similar analysis and identification of time intervals when the QP modulation is observed both in the wave intensity and energetic electron fluxes is done for all the 7 events. The results obtained are shown in Figure 3, which depicts the respective extents in L-shell as a function of the event number. The black vertical lines mark the L-shell extent of individual QP events as seen in the wave data. The red vertical lines mark the L-shell extent of individual QP events as seen in the energetic electron fluxes. The QP modulation of energetic electron fluxes generally occurs in a shorter interval than the QP modulation of wave intensity, and it is located usually toward the higher L-shell edge of the QP event.

Figure 5. Median ratio of energetic electron spectra at the times of the peak fluxes and at the times of preceding/following energetic electron flux minima.

Histograms of L-shells where the events are observed are shown in Figure 4a. These values show how many events span over each particular L-shell bin. The black line corresponds to the QP wave events, while the red line corresponds to the QP modulated energetic electron fluxes. The QP modulation of the wave intensity is typically observed over many L-shells, spanning to low geomagnetic latitudes and at times even all the way to the geomagnetic equator. On the other hand, the QP modulation of energetic electron fluxes is limited to L-shells between about 4 and 6. A histogram of L-shell extents of regions where the QP modulation of energetic electron fluxes is observed is shown in Figure 4b. It can be seen that the typical L-shell extents of these regions are between about 0.6 and 1.2. Additionally, while the QP modulation of the wave intensity for the 7 event orbits is observed in both hemispheres, the QP modulation of energetic electron fluxes is observed in a single hemisphere for each event. This indicates that also the azimuthal extent of the QP modulation of the wave intensity is larger than the azimuthal extent of the QP modulation of energetic electron fluxes. Then, as the spacecraft orbit is generally not confined to a single magnetic meridian (Němec et al., 2010), it can get azimuthally too far from the particular meridian in the conjugate hemisphere to see the QP modulation of energetic electron fluxes. We note that the geomagnetic longitude differences between the locations of the events and the locations where the spacecraft passes through a given L-shell in the conjugate hemisphere range between about 5 and 80 degrees with a median value of about 25 degrees.

The energy spectrum of energetic electrons responsible for the flux peaks is analyzed in Figure 5. In each energy channel, we calculate a ratio of the particle flux at the time of the peak with respect to the flux at the times of the neighboring local minima (i.e., just before and just after the peak). Altogether, 23 flux peaks sufficiently pronounced in the IDP energy spectra data are analyzed. The spectra ratios obtained for individual flux peaks vary quite considerably, among others due to comparatively low resolution of the used IDP spectral data. However, the median ratio of the energy spectra depicted in Figure 5 reveals that the measured fluxes are increased primarily at energies lower than about 250 keV. The maximum median flux increase is about 15%, at an en-

Figure 6. Frequency-estimated source L-shell ranges of individual events. The color coding corresponds to event modulation periods, following the color scale on the right. The dashed curves mark the equatorial electron cyclotron frequency and its half.

Figure 7. A detailed view of the time interval for which the Burst mode data were available (marked by the vertical white lines corresponding to short data gaps in Figure 1). (a) Frequency-time spectrogram of power spectral density of electric field fluctuations measured in the Survey mode resolution. (b) High resolution frequency-time spectrogram of power spectral density of electric field fluctuations obtained using the Burst mode data. (c) Time dependence of the average power spectral density in the frequency range between 1500 and 1750 Hz.

ergy of about 150 keV. Although the median flux ratio gradually decreases toward higher energies, the fluxes appear to remain slightly elevated at energies up to about 500 keV. At higher energies, the median flux ratio starts to fluctuate a lot due to low absolute flux values.

L-shells, where the QP modulation of energetic electron flux is observed, are deemed to correspond to source L-shells of QP events. We thus try to relate event properties to the respective L-shell values, although the available statistics of only 7 events in total is quite a limiting factor. No significant relation between these L-shell values and QP modulation periods is found. However, there appears to be a relation between the L-shell values and QP event frequencies. The corresponding results are shown in Figure 6, which depicts the QP event frequencies as a function of the respective L-shells where the electron precipitation occurs. Each event is depicted by a color rectangle spanning between the minimum and maximum L-shells of QP modulated energetic electron flux and between the minimum and maximum frequencies of the event. The colors of the rectangles correspond to the event modulation periods, following the color scale on the right-hand side. The dashed curves at the upper right part of the figure correspond to equatorial electron cyclotron frequency and half of the equatorial electron cyclotron frequency, respectively. It can be seen that while the QP modulation period does not seem to depend on any of the variables plotted, event frequencies are systematically limited below half of the equatorial electron frequency in the tentative source regions.

The example event from Figures 1 and 2 is exceptional as the spacecraft Burst mode was active for part of the event duration, for about two minutes after 15:35 UT. The measured waveform data allow us to accommodate the parameters of the spectral analysis to get a frequency-time spectrogram with significantly better time resolution than during the Survey mode. Figure 7a shows the Survey mode frequency-time spectrogram of power spectral density of electric field fluctuations, while Figure 7b shows the corresponding frequency-time spectrogram obtained using the Burst mode data. A fast Fourier transform with a length of 4096 data points, 3840 points overlapping, and averaging over 16 neighboring spectra is used, resulting in a time resolution of about 0.1 s and frequency resolution of about 10 Hz. Individual QP elements, in particular the three in the middle of the plotted time interval, are distinguishable in both spectrograms. However, the Burst mode spectrogram reveals an unexpected feature: the QP element intensity does not vary smoothly with time, but it exhibits a fine inner structure. Alternatively, one may describe the situation as discrete emissions with a short repetition period, whose intensity exhibits a slower QP-like modulation. Note that the intense short-lasting emissions observable in Figures 7a and 7b at higher frequencies are lightning generated whistlers, and they are not related to the topic of the present study.

This is further demonstrated in Figure 7c, which shows a time dependence of the average power spectral density in the frequency range between 1500 and 1750 Hz. Intensity modulation with two different periods can be identified. First, it is a slower modulation with a period of about 15 s corresponding to the QP modulation period identifiable in the Survey mode data. Second, it is the faster modulation with a period of about 3.5 s identifiable in the Burst mode data only. This shorter modulation period roughly corresponds to the wave bounce time between the hemispheres (back and forth) at L-shells where QP modulated energetic electron fluxes are observed. For this particular event (event number 5 in Figure 3), the interaction region occurs at somewhat lower L-shells than for other events. Assuming a wave frequency of 1625 Hz, field aligned propagation at $L = 4$, and density dependence along a field line given by Denton et al. (2004), the bounce time is essentially a function of only the equatorial plasma density. In order to obtain bounce times corresponding to the observed modulation period of 3.5 s, one would have to assume the equatorial density of about 225 cm^{-3}. Assuming twice lower/larger plasma number densities would lead to wave bounce times of about 2.6 and 5.0 s, respectively. Such densities are higher than typically observed in the plasma trough (Denton et al., 2004), but they may be possibly justified by a higher density duct region required by the flow cyclotron maser mechanism (Demekhov & Trakhtengerts, 1994). A more typical equatorial plasma trough density of about 50 cm^{-3} would result in a wave bounce time of about 2.0 s.

Finally, multicomponent wave measurements performed at frequencies below 1.25 kHz allow us to perform a detailed wave analysis, i.e., to determine the wave polarization properties and propagation directions (Santolík, Němec, et al., 2006). Although the QP event itself does not extend to such low frequencies, we can possibly assume that the QP elements above about 1.3 kHz propagate in a similar way as the hiss emissions at not too much lower frequencies. The wave analysis (not shown) reveals that the wave magnetic field fluctuations are right-handed nearly circularly polarized. The wave normal angle θ_k is about 45° with respect to the local field line. The wave vector azimuthal angle ϕ_k is close to ±180°, which means that the wave vector stays in the plane of a local magnetic meridian, being deviated from the ambient magnetic field toward lower latitudes. Considering that the event occurs in the northern hemisphere, the observed wave normal direction corresponds to a downward orientation of the wave vector. Such results are consistent with the overall QP propagation survey performed by Hayosh et al. (2016). This propagation, along with the ionospheric reflection taking place (Hanzelka et al., 2017), can account for the larger extent of the wave signatures compared to the particle precipitation. We note, however, that these waves propagating to low latitudes are eventually observable only by spacecraft, as they are generally outside the penetration cone and cannot get to the ground due to the Snell's law (Helliwell, 1965). Wave vector directions close to vertical are needed on the bottom of the ionosphere in order to allow the wave propagation to the ground. This is consistent with conjugate observations of the emissions by spacecraft and ground-based instruments, which indeed reveal the emissions to extend to lower L-shells on board the spacecraft than on the ground (Bezděková et al., 2020).

4 Discussion

Systematic analysis of propagation directions of QP emissions (Němec et al., 2018), as well as prevailing theories of their formation (Demekhov & Trakhtengerts, 1994), suggest that QP emissions are generated in the equatorial region. However, experimental determination of the source radial distance is generally complicated. As the emissions propagate primarily unducted, the L-shells where the QP modulation of the wave intensity is observed do not have to correspond to the L-shells of the source location. Specifically, while the events tend to occupy a considerable portion of the inner magnetosphere, the generation region itself is likely significantly smaller.

Considering that energetic electrons propagate — unlike unducted whistler mode waves — essentially along magnetic field lines, the analysis of energetic electron fluxes related to the event occurrence suppresses the aforementioned complications. The identification of L-shells where the QP modulation of the wave intensity is observed along with the corresponding variations of the energetic electron flux thus allows us to directly determine the L-shell of the interaction region responsible for the observed electron precipitation. However, strictly speaking, the interaction region does not necessarily mean the generation region of the emissions themselves. If the interaction and generation regions were located at different latitudes, then the unducted waves coming from the generation region would eventually reach the interaction region at slightly different L-shells. We also note that, given the low altitude of the DEMETER spacecraft, the measured energetic electrons have very low equatorial pitch angles, being effectively inside or at the edge of the loss cone.

Although more than 2,000 QP emissions identified by Hayosh et al. (2014) are investigated in total, only 7 events with simultaneous QP modulation of the wave intensity and energetic electron fluxes are identified. This can be explained in terms of the spacecraft orbit and used criteria for the event identification. At least three simultaneous peaks in QP wave intensity and electron flux are required for a successful identification. However, at the same time, the events are observed at comparatively large latitudes, where DEMETER sweeps through individual L-shells rather quickly. Considering typical modulation periods of QP events and a limited extent of the interaction region, it is thus possible that for most events DEMETER passes through the corresponding L-shells too quickly to see three subsequent wave intensity/flux peaks. More events would be possibly identified if the condition was relaxed to only two subsequent peaks (or even to a single peak). However, such a condition is deemed not stringent enough, resulting in possible false positive identifications. The aforementioned argumentation necessarily results in a significant selection bias in the identified events. In particular, events with shorter modulation periods and with interaction regions at lower latitudes and spanning over larger latitudinal intervals are more likely to result in a positive identification.

The analysis of L-shells where the QP modulation of energetic electron fluxes is observed reveals that the interaction regions are typically located at L-shells between about 4 and 5, and they span between about 0.6 and 1.2 R_E in the radial distance. This seems to be consistent with former studies which indicated that the source region of the emissions might be located in the equatorial region at larger radial distances (Morrison, 1990; Němec et al., 2018). Considering model plasmapause locations (Moldwin et al., 2002), it seems that although the lower L-shells of the interaction regions are typically not too far from the plasmapause, there is no strict correlation between the model plasmapause locations and the interaction region L-shells. It is, nevertheless, curious that while most interaction regions appear to be located outside the plasmasphere, QP emissions themselves are observed primarily inside the plasmasphere (Němec et al., 2018). This might be possibly explained in terms of the wave propagation between the source region and the observation points, along with the wave trapping and unducted propagation within the plasmasphere similar to the one suggested for chorus-to-hiss mechanism (Church & Thorne, 1983; Chum & Santolík, 2005; Santolík, Chum, et al., 2006; Bortnik et al., 2007, 2008, 2009, 2011; Hartley et al., 2019).

A limited time resolution of the measured energy spectra (4 s) complicates a more detailed analysis of the energies of particles precipitated in relation with QP emissions. However, the results obtained indicate that mostly the particles with energies below about 250 keV are affected. This roughly corresponds to the upper energy in the simulation results (Li et al., 2021). Note that the lower part of the precipitating energetic electron spectrum is not measurable due to the experimental constraints, as the lowest energy channel of the DEMETER IDP instrument is as high as about 72.9 keV. We may try to compare these energies with the first order gyroresonance energies in the interaction regions. Assuming a typical L-shell of 4.5, plasma number density of 25 cm^{-3}, zero pitch angles and field aligned wave vectors, one gets a resonant energy of about 30 keV for the wave frequencies of about 1750 Hz, which is a typical frequency of the analyzed QP events. Note, however, that this is rather a lower estimate of the first order gyroresonance energy; oblique wave vectors at the equator would lead to higher resonant energies. Nevertheless, the first order gyroresonance energy stays below the observed precipitation energies unless a significantly lower equatorial plasma number density is assumed (< 10 cm^{-3}). Note also that we assume the North-South symmetry: the interacting waves would propagate to the opposite hemisphere than the precipitating electrons. For completeness, we remark that the Landau resonance energy is only about 5% of the first order gyroresonance energy, i.e., well below the energies of the observed precipitating electrons.

The upper frequency limit on the QP emissions, corresponding to half of the equatorial electron cyclotron frequency, is in agreement with former studies based purely on wave observations, not on the particle observations (Němec et al., 2018). Considering that the half of the equatorial electron cyclotron frequency corresponds to the upper frequency limit for the wave ducting in density crest ducts (R. L. Smith, 1961), this observation can be considered as an indirect supporting evidence for the flow cyclotron maser theory of the emission formation (Demekhov & Trakhtengerts, 1994). The wave bouncing back and forth between the hemispheres, assumed by this theory, would be further in line with the fine structure of individual QP elements revealed by the high resolution Burst mode data. We note that the fine temporal structure corresponding to the whistler wave hop time is in agreement with some QP emissions observed on the ground (Manninen, Demekhov, et al., 2014). We also note that, unlike in the case of multihop whistlers, the wave elements do not become less intense or more dispersed at later times of the event. This seems consistent with the bouncing wave elements reported by Němec et al. (2009) using conjugate ground-based and satellite observations. It might be perhaps understood in terms of the wave element intensity and spectral shape not being governed simply by the propagation and dispersion, but rather by the wave-particle interactions taking place in the source region.

5 Conclusions

A set of QP emissions identified during the entire DEMETER spacecraft mission is used to check for simultaneous variations of the wave intensity and energetic electron fluxes. Only 7 events out of more than 2,000 events investigated in total exhibit such simultaneous variations. This may be explained by observational restraints, as at least three simultaneous peaks of the wave intensity and flux are needed for a positive identification, requiring the region to be sufficiently extended in L-shell and the modulation period being not too large. The observed energetic electron flux modulations are found to occur primarily at energies lower than about 250 keV.

The time intervals when the QP modulation of the energetic electron flux is observed are interpreted as the spacecraft crossing the magnetic field lines going through the generation region of the emissions. Energetic particle fluxes are in this sense a better tracer of the source location, as they — unlike unducted propagating whistler mode waves — may be regarded as propagating strictly along the magnetic field lines. Despite the low number of events and the clear selection bias present, we can thus estimate the locations and radial dimensions of the anticipated generation regions. They are found to be at L-shells between about 4 and 6, with the respective source radial dimensions being about 0.6 to 1.2 R_E. The event frequencies are generally confined below half of the equatorial electron gyrofrequency in these regions.

Finally, high resolution wave measurements available during the spacecraft Burst mode for one of the events revealed that the individual QP elements exhibit a fine inner structure. They are composed of faster repeating elements, with the period corresponding to the wave bouncing along the magnetic field line between the hemispheres.

Our results provide important experimental constraints for mechanisms suggested to explain the formation of QP emissions.

Acknowledgments

We thank the engineers from CNES and scientific laboratories (CBK, IRAP, LPC2E, LPP, and SSD of ESTEC) who largely contributed to the success of the DEMETER mission. DEMETER data are accessible from the https://sipad-cdpp.cnes.fr website. F. N. and O. S. acknowledge the support of GACR Grant 21-01813S. The work of M. H. and O. S. on the present paper has received funding from the European Union's Horizon 2020 research and innovation programme under grant agreement No. 870437 (SafeSpace).

References

Berthelier, J. J., Godefroy, M., Leblanc, F., Malingre, M., Menvielle, M., Lagoutte, D., . . . Pfaff, R. (2006). ICE, the electric field experiment on DEMETER. *Planet. Space Sci.*, *54*, 456–471. doi: 10.1016/j.pss.2005.10.016

Bezděková, B., Němec, F., Manninen, J., Hospodarsky, G. B., Santolík, O., Kurth, W. S., & Hartley, D. P. (2020). Conjugate observations of quasiperiodic emissions by the Van Allen Probes spacecraft and ground-based station Kannuslehto. *J. Geophys. Res. Space Physics*, *125*(e2020JA027793). doi: 10.1029/2020JA027793

Bezděková, B., Němec, F., Parrot, M., Hajoš, M., Záhlava, J., & Santolík, O. (2019). Dependence of properties of magnetospheric line radiation and quasiperiodic emissions on solar wind parameters and geomagnetic activity. *JGRSPACE*, *124*, 2552–2568. doi: 10.1029/2018JA026378

Bortnik, J., Chen, L., Li, W., Thorne, R. M., & Horne, R. B. (2011). Modeling the evolution of chorus waves into plasmaspheric hiss. *J. Geophys. Res.*, *116*(A08221). doi: 10.1029/2011JA016499

Bortnik, J., Li, W., Thorne, R. M., Angelopoulos, V., Cully, C., Bonnell, J., ... Roux, A. (2009). An observation linking the origin of plasmaspheric hiss to discrete chorus emissions. *Science*, *324*, 775–778. doi: 10.1126/science.1171273

Bortnik, J., Thorne, R. M., & Meredith, N. P. (2008). The unexpected origin of plasmaspheric hiss from discrete chorus emissions. *Nature*, *452*, 62–66. doi: 10.1038/nature06741

Bortnik, J., Thorne, R. M., Meredith, N. P., & Santolík, O. (2007). Ray tracing of penetrating chorus and its implications for the radiation belts. *Geophys. Res. Lett.*, *34*(L15109). doi: 10.1029/2007GL030040

Carson, W. B., Koch, J. A., Pope, J. H., & Gallet, R. M. (1965). Long-period very low frequency emission pulsations. *J. Geophys. Res.*, *70*(17), 4293–4303. doi: 10.1029/JZ070i017p04293

Chen, L. (1974). Theory of ULF modulation of VLF emissions. *Geophys. Res. Lett.*, *1*(2), 73–75. doi: 10.1029/GL001i002p00073

Chum, J., & Santolík, O. (2005). Propagation of whistler-mode chorus to low altitudes: Divergent ray trajectories and ground accessibility. *Ann. Geophys.*, *23*, 3727–3738. doi: 10.5194/angeo-23-3727-2005

Church, S. R., & Thorne, R. M. (1983). On the origin of plasmaspheric hiss: Ray path integrated amplification. *J. Geophys. Res.*, *88*(A10), 7941–7957. doi: 10.1029/JA088iA10p07941

Demekhov, A. G., & Trakhtengerts, V. Y. (1994). A mechanism of formation of pulsating aurorae. *J. Geophys. Res.*, *99*(A4), 5831–5841. doi: 10.1029/93JA01804

Denton, R. E., Takahashi, K., Anderson, R. R., & Wuest, M. P. (2004). Magnetospheric toroidal Alfvén wave harmonics and the field line distribution of mass density. *J. Geophys. Res.*, *109*(A06202). doi: 10.1029/2003JA010201

Engebretson, M. J., Posch, J. L., Halford, A. J., Shelburne, G. A., Smith, A. J., Spasojević, M., ... Arnoldy, R. L. (2004). Latitudinal and seasonal variations of quasiperiodic and periodic VLF emissions in the outer magnetosphere. *J. Geophys. Res.*, *109*(A05216). doi: 10.1029/2003JA010335

Hanzelka, M., Santolík, O., Hajoš, M., Němec, F., & Parrot, M. (2017). Observation of ionospherically reflected quasiperiodic emissions by the DEMETER spacecraft. *Geophys. Res. Lett.*, *44*, 8721–8729. doi: 10.1002/2017GL074883

Hartley, D. P., Kletzing, C. A., Chen, L., Horne, R. B., & Santolík, O. (2019). Van Allen Probes observations of chorus wave vector orientations: Implications for the chorus-to-hiss mechanism. *Geophys. Res. Lett.*, *46*, 2337–2346. doi: 10.1029/2019GL082111

Hayosh, M., Němec, F., Santolík, O., & Parrot, M. (2014). Statistical investigation of VLF quasiperiodic emissions measured by the DEMETER spacecraft. *J. Geophys. Res. Space Physics*, *119*, 8063–8072. doi: 10.1002/2013JA019731

Hayosh, M., Němec, F., Santolík, O., & Parrot, M. (2016). Propagation properties of quasi-periodic VLF emissions observed by the DEMETER spacecraft. *J. Geophys. Res. Space Physics*, *43*, 1007–1014. doi: 10.1002/2015GL067373

Hayosh, M., Pasmanik, D. L., Demekhov, A. G., Santolík, O., Parrot, M., & Titova, E. E. (2013). Simultaneous observations of quasi-periodic ELF/VLF wave emissions and electron precipitation by DEMETER satellite. a case study. *J. Geophys. Res. Space Physics*, *118*, 4523–4533. doi: 10.1002/jgra.50179

Helliwell, R. A. (1965). *Whistlers and related ionospheric phenomena.* Stanford, Calif.: Stanford University Press.

Kimura, I. (1974). Interrelation between VLF and ULF emissions. *Space Sci. Rev.*, *16*, 389–411. doi: 10.1007/BF00171565

Kitamura, T., Jacobs, J. A., Watanabe, T., & R. B. Flint, J. (1969). An investigation of quasi-periodic VLF emissions. *J. Geophys. Res.*, *74*(24), 5652–5664. doi: 10.1029/JA074i024p05652

Li, J., Bortnik, J., Ma, Q., Li, W., Shen, X., Nishimura, Y., ... Baker, D. N. (2021). Multipoint observations of quasiperiodic emission intensification and effects on energetic electron precipitation. *J. Geophys. Res. Space Physics*, *126*(e2020JA028484). doi: 10.1029/2020JA028484

Manninen, J., Demekhov, A. G., Titova, E. E., Kozlovsky, A. E., & Pasmanik, D. L. (2014). Quasiperiodic VLF emissions with short-period modulation and their relationship to whistlers: A case study. *J. Geophys. Res. Space Physics*, *119*, 3544-3557. doi: 10.1002/2013JA019743

Manninen, J., Kleimenova, N. G., & Kozyreva, O. V. (2012). New type of ensemble of quasi-periodic, long-lasting VLF emissions in the auroral zone. *Ann. Geophys.*, *30*, 1655-1660. doi: 10.5194/angeo-30-1655-2012

Manninen, J., Kleimova, N. G., Kozyreva, O. V., Bespalov, P. A., & Kozlovsky, A. E. (2013). Non-typical ground-based quasi-periodic VLF emissions observed at $L \sim 5.3$ under quiet geomagnetic conditions at night. *J. Atm. Solar-Terr. Phys.*, *99*, 123–128. doi: 10.1016/j.jastp.2012.05.007

Manninen, J., Titova, E. E., Demekhov, A. G., Kozlovskii, A. E., & Pasmanik, D. L. (2014). Quasiperiodic VLF emissions: Analysis of periods on different timescales. *Cosmic Research*, *52*(1), 61–67. doi: 10.1134/S0010952514010055

Martinez-Calderon, C., Shiokawa, K., Miyoshi, Y., Keika, K., Ozaki, M., Schofield, I., . . . Kurth, W. S. (2016). ELF/VLF wave propagation at subauroral latitudes: Conjugate observation between the ground and Van Allen Probes A. *J. Geophys. Res. Space Physics*, *121*. doi: 10.1002/2015JA022264

Moldwin, M. O., Downward, L., Rassoul, H. K., Amin, R., & Anderson, R. R. (2002). A new model of the location of the plasmapause: CRRES results. *J. Geophys. Res.*, *107*(A11). doi: 10.1029/2001JA009211

Morrison, K. (1990). Quasi-periodic VLF emissions and concurrent magnetic pulsations seen at $L = 4$. *Planet. Space Sci.*, *38*(12), 1555-1565. doi: 10.1016/0032-0633(90)90161-I

Morrison, K., Engebretson, M. J., Beck, J. R., Johnson, J. E., Arnoldy, R. L., L. J. Cahill, J., . . . Gallani, M. (1994). A study of quasi-periodic ELF-VLF emissions at three antarctic stations: Evidence for off-equatorial generation? *Ann. Geophys.*, *12*, 139–146. doi: 10.1007/s00585-994-0139-8

Němec, F., Bezděková, B., Manninen, J., Parrot, M., Santolík, O., Hayosh, M., & Turunen, T. (2016). Conjugate observations of a remarkable quasiperiodic event by the low-altitude DEMETER spacecraft and ground-based instruments. *J. Geophys. Res. Space Physics*, *121*, 8790–8803. doi: 10.1002/2016JA022968

Němec, F., Hospodarsky, G., Pickett, J. S., Santolík, O., Kurth, W. S., & Kletzing, C. (2016). Conjugate observations of quasiperiodic emissions by the Cluster, Van Allen Probes, and THEMIS spacecraft. *J. Geophys. Res. Space Physics*, *121*, 7647–7663. doi: 10.1002/2016JA022774

Němec, F., Hospodarsky, G. B., Bezděková, B., Demekhov, A. G., Pasmanik, D. L., Santolík, O., ... Hartley, D. (2018). Quasiperiodic whistler mode emissions observed by the Van Allen Probes spacecraft. *J. Geophys. Res. Space Physics*, *123*, 8969–8982. doi: 10.1029/2018JA026058

Němec, F., Pickett, J. S., & Santolík, O. (2014). Multispacecraft Cluster observations of quasiperiodic emissions close to the geomagnetic equator. *J. Geophys. Res. Space Physics*, *119*, 9101–9112. doi: 10.1002/2014JA020321

Němec, F., Raita, T., Parrot, M., Santolík, O., & Turunen, T. (2009). Conjugate observations on board a satellite and on the ground of a remarkable MLR-like event. *Geophys. Res. Lett.*, *36*(L22103). doi: 10.1029/2009GL040974

Němec, F., Santolík, O., Hospodarsky, G. B., Hajoš, M., Demekhov, A. G., Kurth, W. S., ... Hartley, D. P. (2020). Whistler mode quasiperiodic emissions: Contrasting Van Allen Probes and DEMETER occurrence rates. *J. Geophys. Res. Space Physics*, *125*(e2020JA027918). doi: 10.1029/2020JA027918

Němec, F., Santolík, O., Parrot, M., Pickett, J. S., Hayosh, M., & Cornilleau-Wehrlin, N. (2013). Conjugate observations of quasi-periodic emissions by Cluster and DEMETER spacecraft. *J. Geophys. Res. Space Physics*, *118*, 198–208. doi: 10.1029/2012JA018380

Němec, F., Santolík, O., Parrot, M., & Rodger, C. J. (2010). Relationship between median intensities of electromagnetic emissions in the VLF range and lightning activity. *J. Geophys. Res.*, *115*(A08315). doi: 10.1029/2010JA015296

Němec, F., Santolík, O., Pickett, J. S., Parrot, M., & Cornilleau-Wehrlin, N. (2013). Quasiperiodic emissions observed by the Cluster spacecraft and their association with ULF magnetic pulsations. *J. Geophys. Res. Space Physics*, *118*, 4210–4220. doi: 10.1002/jgra.50406

Parrot, M., Benoist, D., Berthelier, J. J., Blecki, J., Chapuis, Y., Colin, F., ... Zamora, P. (2006). The magnetic field experiment IMSC and its data processing onboard DEMETER: Scientific objectives, description and first results. *Planet. Space Sci.*, *54*, 441–455. doi: 10.1016/j.pss.2005.10.015

Pasmanik, D. L., Demekhov, A. G., Hayoš, M., Němec, F., Santolík, O., & Parrot, M. (2019). Quasiperiodic ELF/VLF emissions detected onboard the DEMETER spacecraft: Theoretical analysis and comparison with observations. *J. Geophys. Res. Space Physics*, *124*, 5278–5288. doi: 10.1029/2018JA026444

Pasmanik, D. L., Demekhov, A. G., Trakhtengerts, V. Y., & Parrot, M. (2004). Modeling whistler wave generation regimes in magnetospheric cyclotron maser. *Ann. Geophys.*, *22*, 3561–3570. doi: 10.5194/angeo-22-3561-2004

Pasmanik, D. L., Titova, E. E., Demekhov, A. G., Trakhtengerts, V. Y., Santolik, O., Jiricek, F., … Parrot, M. (2004). Quasi-periodic ELF/VLF wave emissions in the Earth's magnetosphere: Comparison of satellite observations and modelling. *Ann. Geophys.*, *22*, 4351–4361. doi: 10.5194/angeo-22-4351-2004

Santolík, O., Chum, J., Parrot, M., Gurnett, D. A., Pickett, J. S., & Cornilleau-Wehrlin, N. (2006). Propagation of whistler mode chorus to low altitudes: Spacecraft observations of structured ELF hiss. *J. Geophys. Res.*, *111*(A10208). doi: 10.1029/2005JA011462

Santolík, O., Němec, F., Parrot, M., Lagoutte, D., Madrias, L., & Berthelier, J. J. (2006). Analysis methods for multi-component wave measurements on board the DEMETER spacecraft. *Planet. Space Sci.*, *54*, 512–527. doi: 10.1016/j.pss.2005.10.020

Santolík, O., Parrot, M., & Lefeuvre, F. (2003). Singular value decomposition methods for wave propagation analysis. *Radio Sci.*, *38*(1). doi: 10.1029/2000RS002523

Sato, N., Hayashi, K., Kokubun, S., Oguti, T., & Fukunishi, H. (1974). Relationships between quasi-periodic VLF emission and geomagnetic pulsation. *J. Atm. and Terr. Phys*, *36*, 1515–1526. doi: 10.1016/0021-9169(74)90229-3

Sato, N., & Kokubun, S. (1980). Interaction between ELF-VLF emissions and magnetic pulsations: Quasi-periodic ELF-VLF emissions associated with Pc 3-4 magnetic pulsations and their geomagnetic conjugacy. *J. Geophys. Res.*, *85*(A1), 101–113. doi: 10.1029/JA085iA01p00101

Sato, N., & Kokubun, S. (1981). Interaction between ELF-VLF emissions and magnetic pulsations: Regular period ELF-VLF pulsations and their geomagnetic conjugacy. *J. Geophys. Res.*, *86*(A1), 9–18. doi: 10.1029/JA086iA01p00009

Sato, N., & Matsudo, T. (1986). Origin of magnetic pulsations associated with regular period VLF pulsations (Type 2 QP) observed on the ground at Syowa Station. *J. Geophys. Res.*, *91*(A10), 11,179–11,185. doi: 10.1029/JA091iA10p11179

Sauvaud, J. A., Moreau, T., Maggiolo, R., Treilhou, J.-P., Jacquey, C., Cros, A., ... Gangloff, M. (2006). High-energy electron detection onboard DEMETER: The IDP spectrometer, description and first results on the inner belt. *Planet. Space Sci.*, *54*, 502–511. doi: 10.1016/j.pss.2005.10.019

Sazhin, S. S. (1987). An analytical model of quasiperiodic ELF-VLF emissions. *Planet. Space Sci.*, *35*(10), 1267-1274. doi: 10.1016/0032-0633(87)90111-5

Sazhin, S. S., & Hayakawa, M. (1994). Periodic and quasiperiodic VLF emissions. *J. Geophys. Res.*, *56*(6), 735–753. doi: 10.1016/0021-9169(94)90130-9

Smith, A. J., Engebretson, M. J., Klatt, E. M., Inan, U. S., Arnoldy, R. L., & Fukunishi, H. (1998). Periodic and quasiperiodic ELF/VLF emissions observed by an array of Antarctic stations. *J. Geophys. Res.*, *103*(A10), 23,611–23,622. doi: 10.1029/98JA01955

Smith, R. L. (1961). Propagation characteristics of whistlers trapped in field-aligned columns of enhanced ionization. *J. Geophys. Res.*, *66*(11), 3699–3707. doi: 10.1029/JZ066i011p03699

Titova, E. E., Kozelov, B. V., Demekhov, A. G., Manninen, J., Santolík, O., Kletzing, C. A., & Reeves, G. (2015). Identification of the source of quasiperiodic VLF emissions using ground-based and van allen probes satellite observations. *Geophys. Res. Lett.*, *42*, 6137–6145. doi: 10.1002/2015GL064911

Tixier, M., & Cornilleau-Wehrlin, N. (1986). How are the VLF quasi-periodic emissions controlled by harmonics of field line oscillations? The results of a comparison between ground and GEOS satellites measurements. *J. Geophys. Res.*, *91*(A6), 6899–6919. doi: 10.1029/JA091iA06p06899

Trakhtengerts, V. Y., & Rycroft, M. J. (2008). Whistler and Alfvén mode cyclotron masers in space. In (p. 354). Cambridge University Press. doi: 10.1017/CBO9780511536519

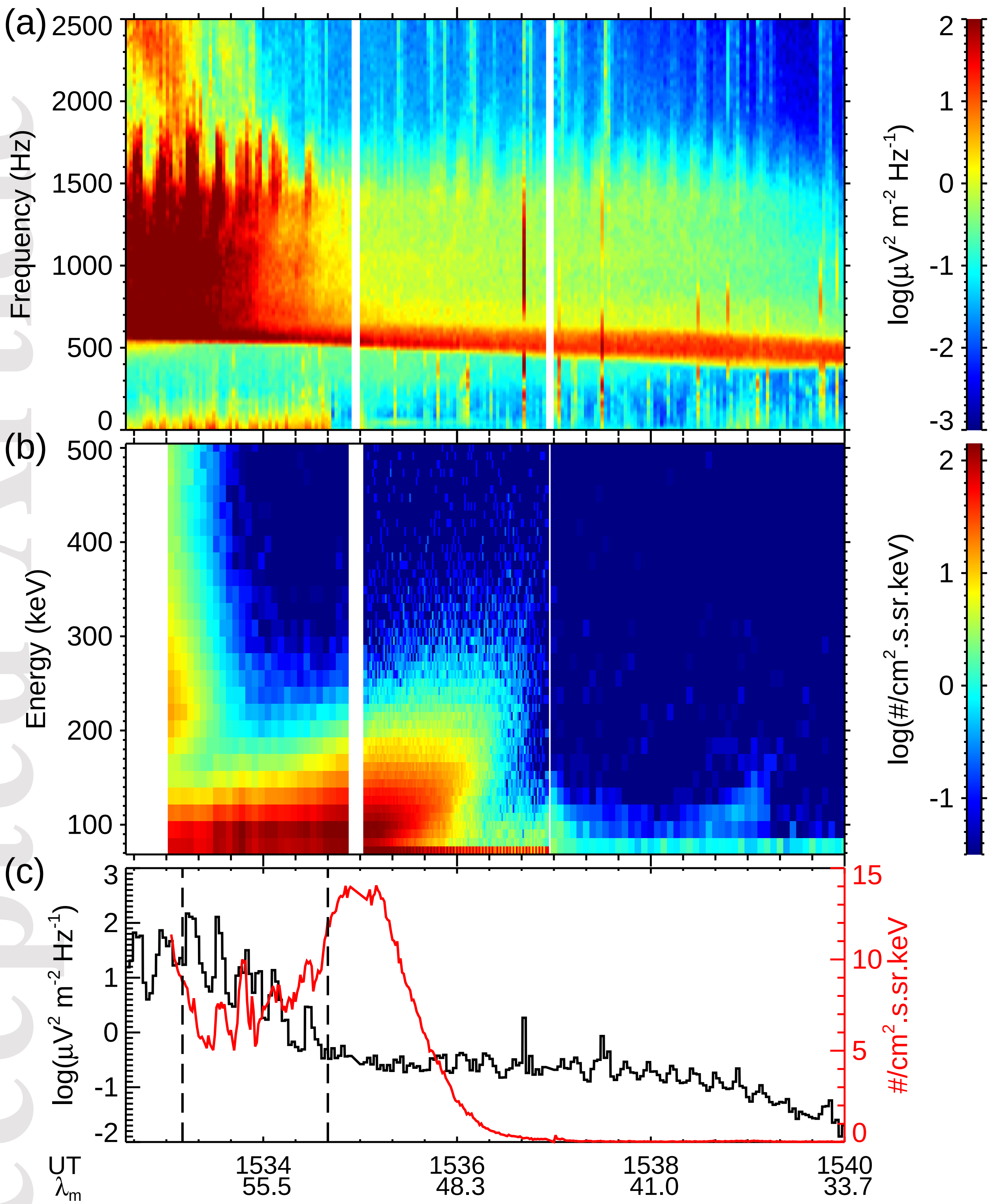

(a)
2500
2000
1500
1000
500
0
Frequency (Hz)
2
1
0
-1
-2
-3
log(µV² m⁻² Hz⁻¹)
(b)
500
400
300
200
100
Energy (keV)
2
1
0
-1
log(#/cm².s.sr.keV)
(c)
3
2
1
0
-1
-2
log(µV² m⁻² Hz⁻¹)
15
10
5
0
#/cm².s.sr.keV
UT
λm
1534
55.5
1536
48.3
1538
41.0
1540
33.7

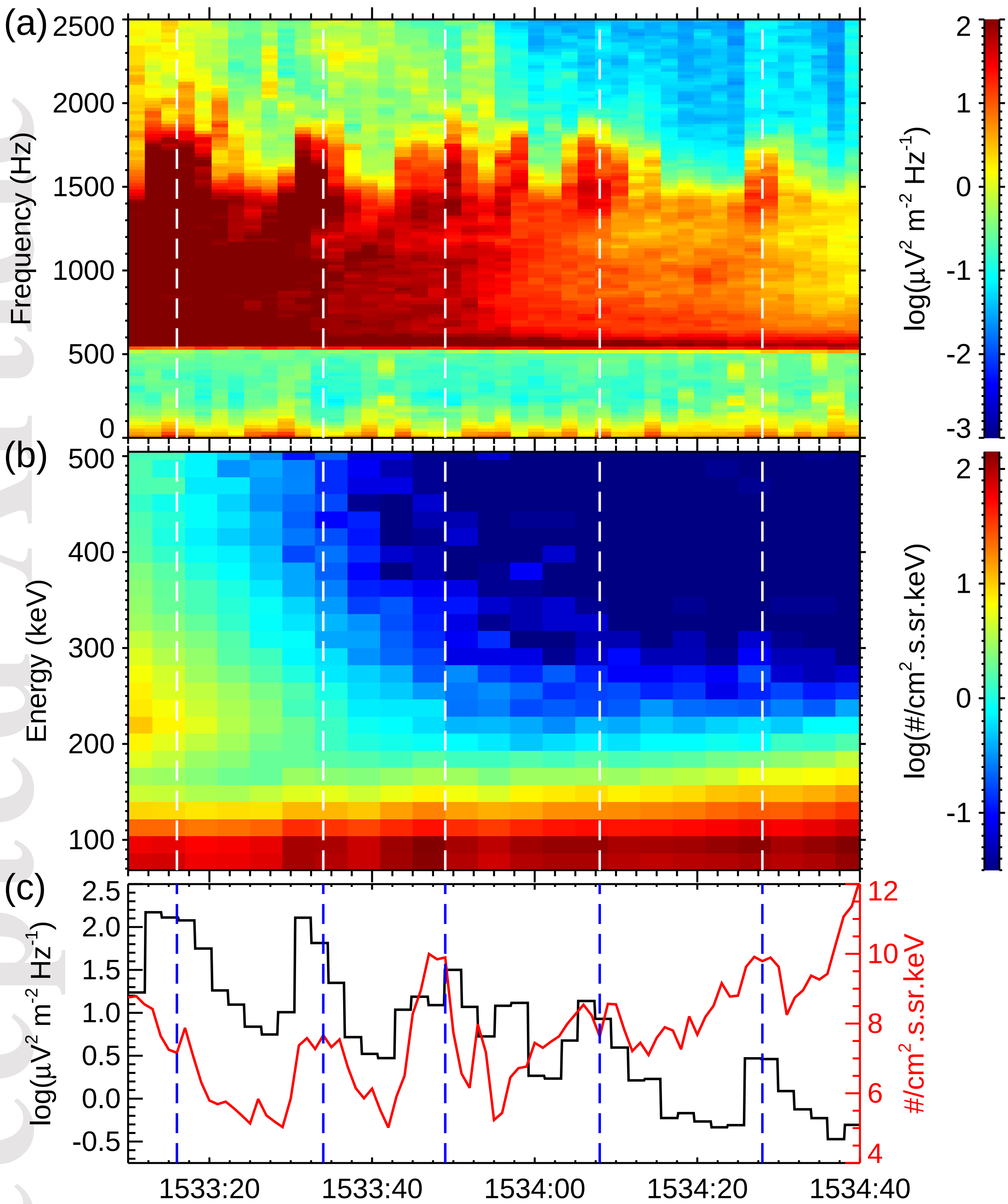
(a)
(b)
(c)
Frequency (Hz)
Energy (keV)
log(µV² m⁻² Hz⁻¹)
log(#/cm².s.sr.keV)
#/cm².s.sr.keV
1533:20
1533:40
1534:00
1534:20
1534:40

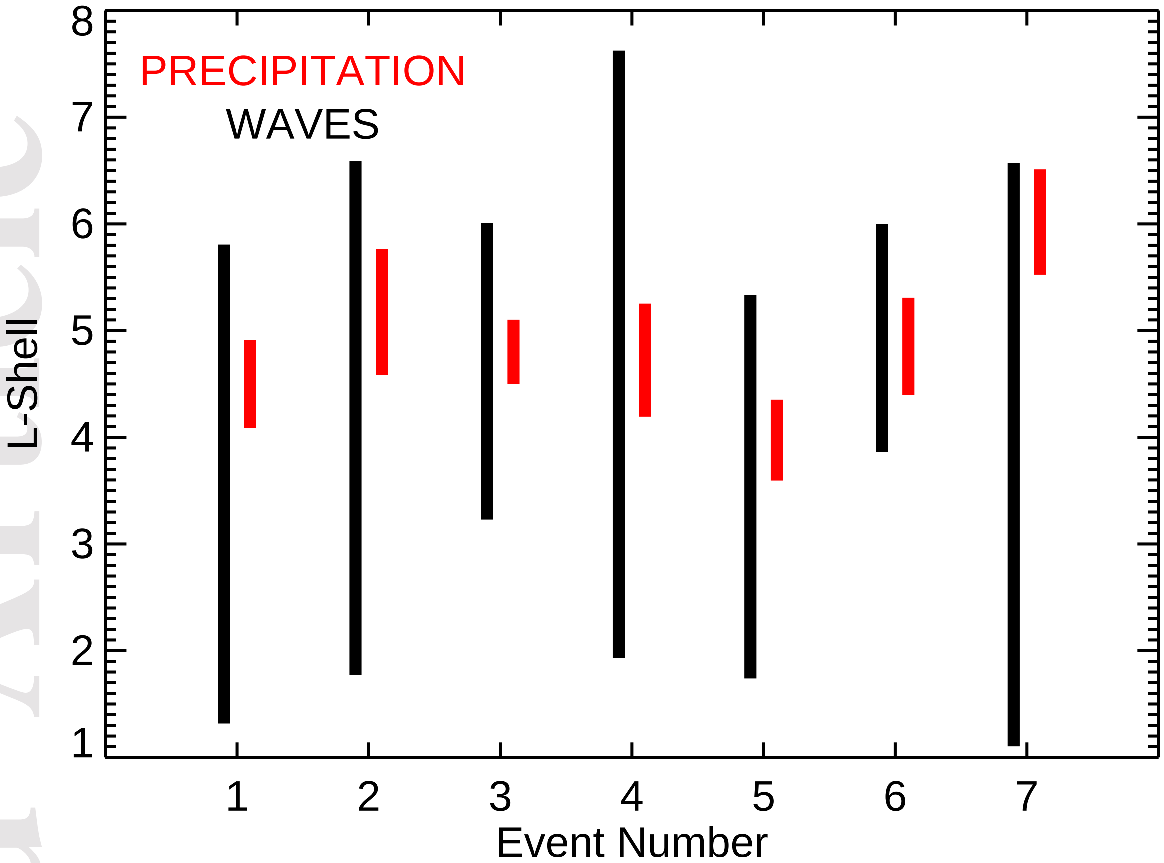
PRECIPITATION
WAVES
L-Shell
8
7
6
5
4
3
2
1
1
2
3
4
5
6
7
Event Number

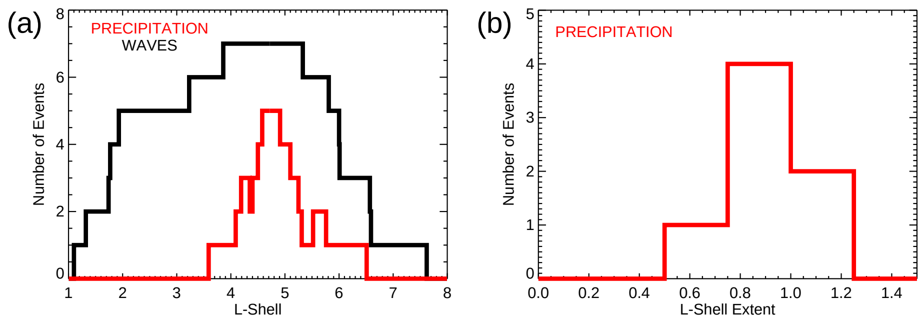
(a)
PRECIPITATION
WAVES
Number of Events
L-Shell
(b)
PRECIPITATION
Number of Events
L-Shell Extent

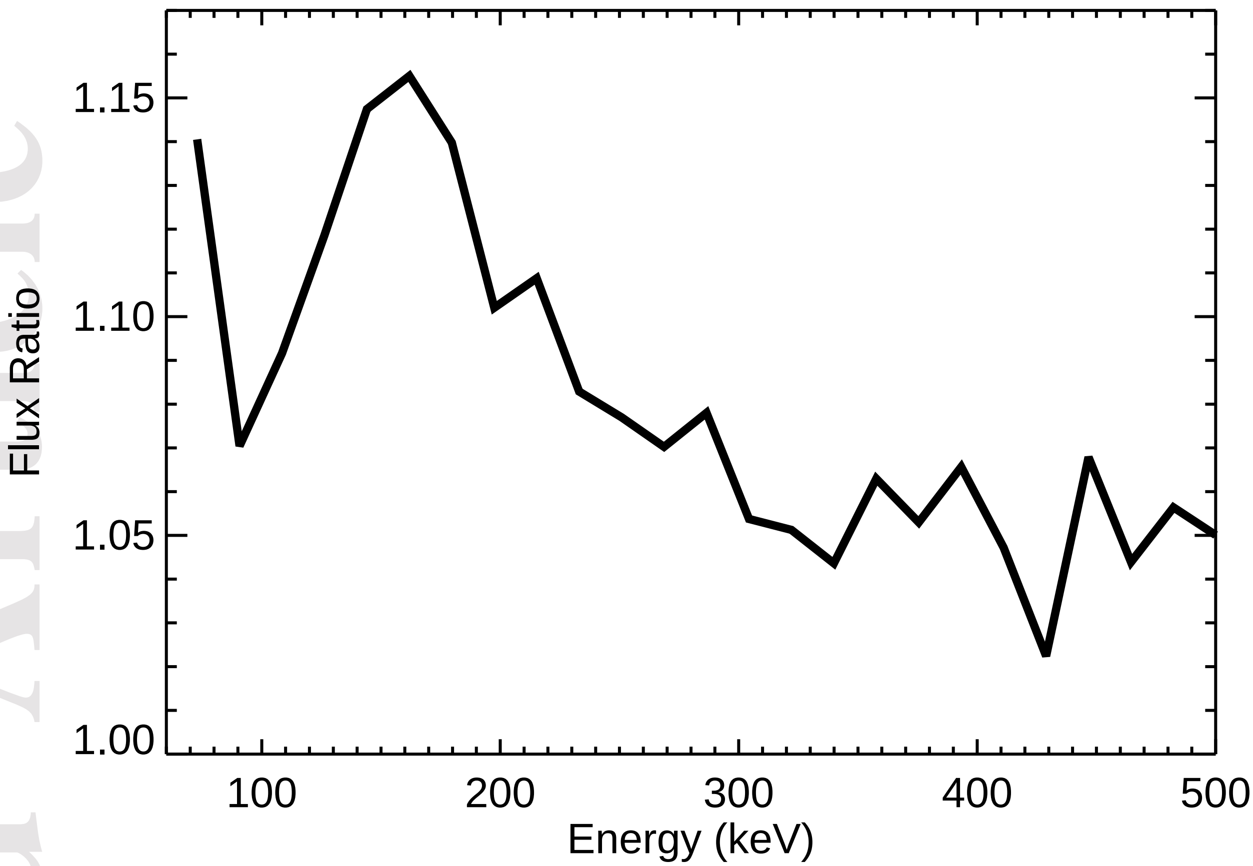
1.15
1.10
1.05
1.00
Flux Ratio
100
200
300
400
500
Energy (keV)

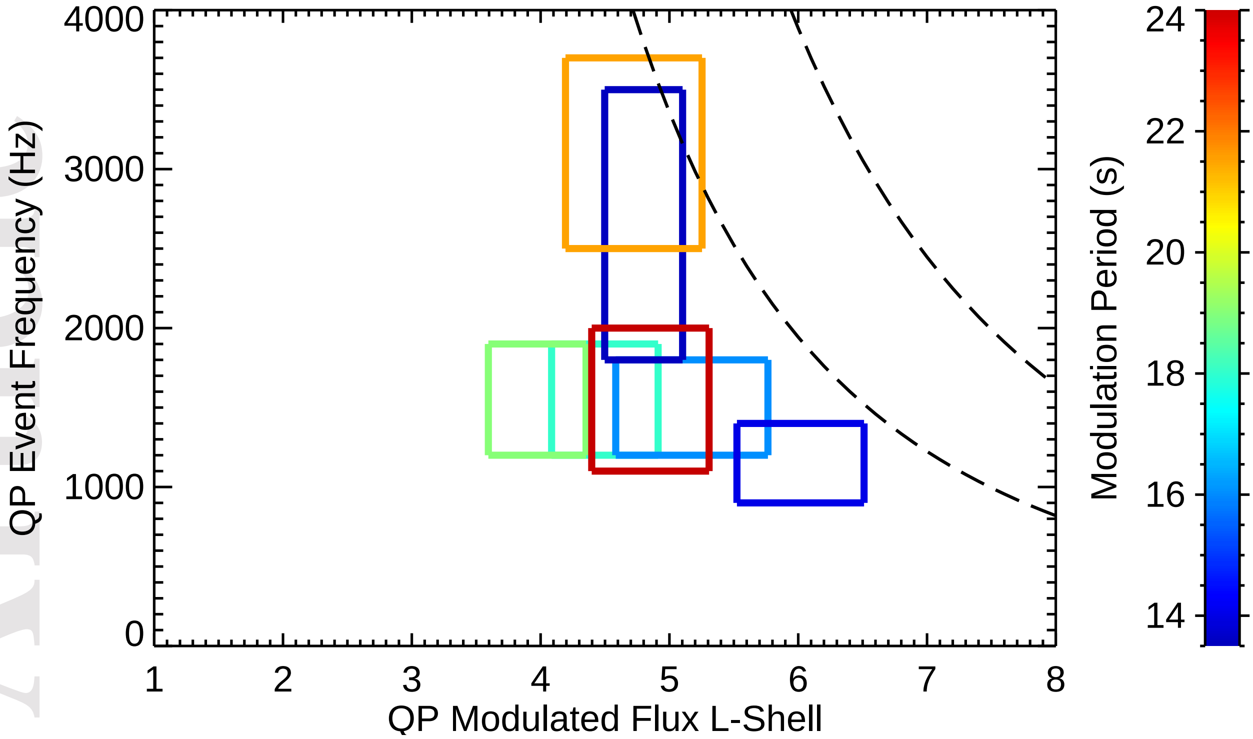
4000
3000
2000
1000
0
QP Event Frequency (Hz)
1
2
3
4
5
6
7
8
QP Modulated Flux L-Shell
24
22
20
18
16
14
Modulation Period (s)

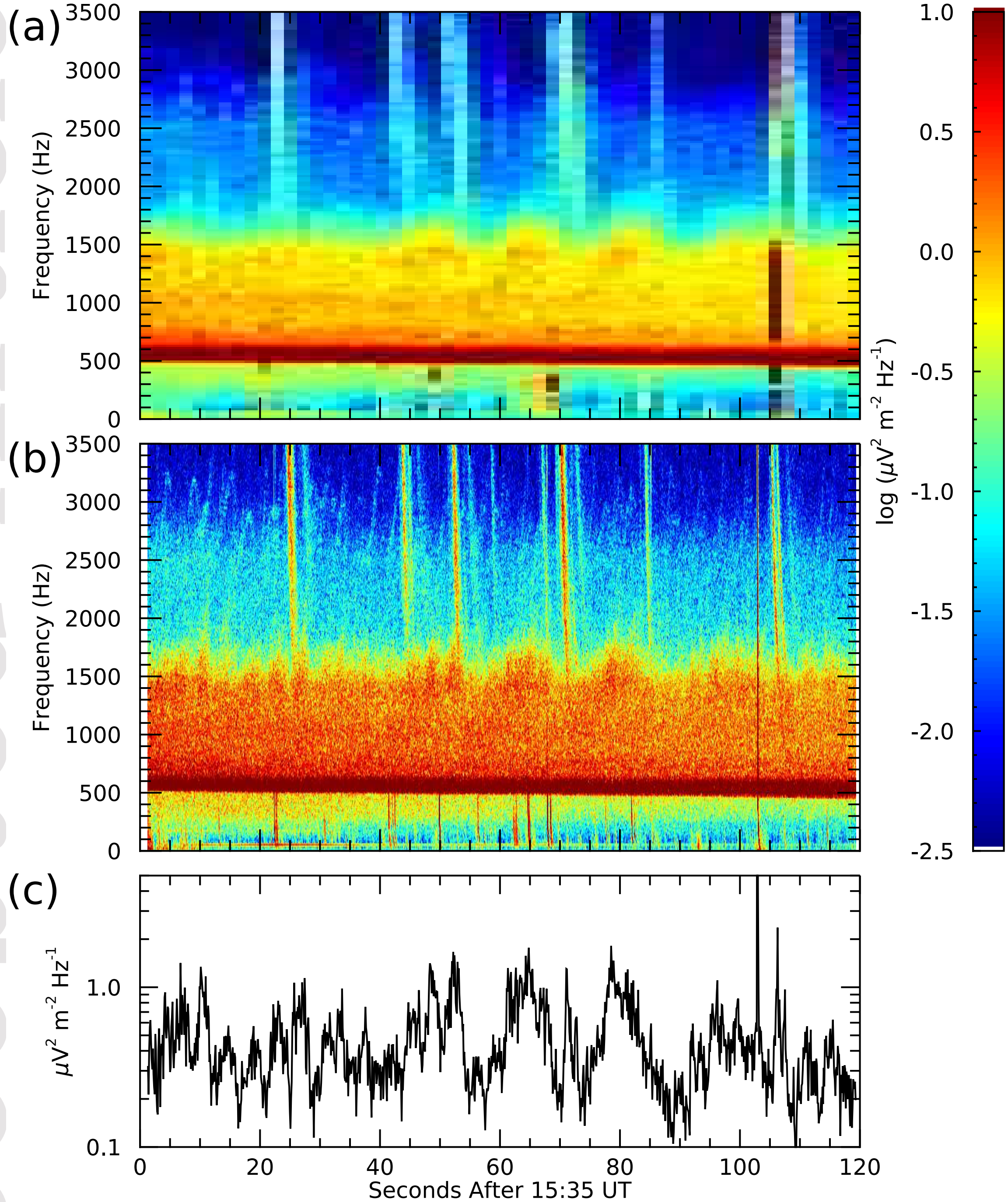
(a)
(b)
(c)
Frequency (Hz)
3500
3000
2500
2000
1500
1000
500
0
1.0
0.5
0.0
-0.5
-1.0
-1.5
-2.0
-2.5
log (μV^2 m^{-2} Hz^{-1})
μV^2 m^{-2} Hz^{-1}
1.0
0.1
0
20
40
60
80
100
120
Seconds After 15:35 UT